



OPEN

Spatiotemporal characterization of heatwave exposure across historically vulnerable communities

Saurav Bhattarai^{1✉}, Sunil Bista¹, Sanjib Sharma², Loren D. White³, Farshad Amini¹ & Rocky Talchabhadel¹

Heatwaves pose a serious threat and are projected to amplify with changing climate and social demographics. A comprehensive understanding of heatwave exposure to the communities is imperative for the development of effective strategies and mitigation plans. This study explores spatiotemporal characterization of heatwaves across the historically vulnerable communities in Mississippi, United States. We derive multiple heatwave metrics including frequency, duration, and magnitude based on temperature data for urban-specific daytime, nighttime, and day–night combined conditions. Our analysis depicts a rising heatwave trend across all counties, with the most extreme shifts observed in prolonged day–night events lacking overnight relief. We integrate physical heatwave hazards with a socioeconomic vulnerability index to develop an integrated urban heatwave risk index. Integrated metric identifies the counties in northwest Mississippi as heat-prone areas, exhibiting an urgent need to prioritize heat resilience and adaptive strategies in these regions. The compounding urban heatwave and vulnerability risks in these communities highlights an environmental justice imperative to implement equitable policies that protect disadvantaged populations. Although this study is focused on Mississippi, our framework is scalable and can be employed to urban regions globally. This study provides a solid foundation for developing timely heatwave preparedness and mitigation to avert preventable heat-related tragedies as extremes intensify with climate change.

Keywords Heatwave, Climate change, Social vulnerability, Integrated heatwave risk index, Mississippi

Heatwaves, defined as extended periods of excessive heat, have become more frequent and damaging across the world¹. From 1998 to 2017, climate disasters caused over \$2 trillion in cumulative global economic losses, with extreme heat being among the deadliest and costliest natural hazards^{2,3}. This intensification has led to severe environmental and societal impacts, including increased cardiovascular mortality^{4,5}, hospital admissions for heat-related or heat-adjacent illness^{5–10}, urban heat island effects^{11,12}, intense droughts^{13,14}. Over the past four decades, temperatures have risen 1–2 °C globally as the frequency of heatwaves has tripled across several parts of the world^{15–18}. Future projections indicate that the global average temperature in 2100 could rise by 5.4 °C than it is in 2022⁴. Between 1998 and 2017, over 150,000 deaths resulted from heat waves¹⁹. Currently 30% of the global population is exposed to such extreme heat which is expected to intensify further by 2100^{20,21}. Urgent action is needed to protect vulnerable communities from the rising threat of extreme heat events, which are becoming more frequent, intense, and prolonged across the globe^{1,22,23}.

Excessive heat is one of the leading causes of climate-related death and economic losses in the USA^{5,24–28}. Heatwaves have risen approximately 0.75 and 0.4 events per decade based on minimum and maximum temperatures, respectively, while contributing 8.6 and 5.2 more days per decade²⁹. Over 11,000 Americans died from heatwaves between 1979 and 2018³⁰. In 2020, heatwave-related infrastructure repair costs exceeded \$1 billion in several states. Nationwide road maintenance may exceed \$25 billion by 2040^{31,32}. Annual heat-induced labor productivity losses amount to around \$100 billion, which is equivalent to the combined budgets of Homeland

¹Department of Civil and Environmental Engineering, Jackson State University, Jackson, MS, USA. ²Department of Civil and Environmental Engineering, Howard University, Washington, DC, USA. ³Department of Chemistry, Physics, and Atmospheric Sciences, Jackson State University, Jackson, MS, USA. ✉email: saurav.bhattarai@students.jsums.edu

Security, and Housing and Urban Development^{22,33}. This aligns with calculations showing that in the USA, the loss of work capacity in moderate level work in the shade will increase from 0.17% now to more than 1.3% at the end of the century based on projected temperature increases³⁴. Other research estimates that rising temperatures could lead to 1.5–4.4 billion lost workforce hours and \$51–119 billion in economic losses in the USA by 2100³⁵.

High temperatures and prolonged heatwaves during crop growing seasons have stressed crops and reduced yield²². These losses have had a profound impact on the agricultural industry and have far-reaching effects on food prices, availability, and the overall country's economy^{22,29,33}. Heatwave impacts can increase in the future with changing climatic conditions and global warming³⁶. By 2050, annual labor losses are projected to reach \$500 billion, crop yields to decline 10–13%, and deaths rise over six-fold²². Heatwaves have disproportionately affected regions and demographics across the USA^{22,37}. Minorities and low-income populations tend to suffer more heat-related health impacts^{37,38}. Black and African American individuals are 34–41% more likely to be affected with the highest increases in childhood asthma diagnoses than other groups under 2–4 °C of global warming³⁹. Hispanics and Latinos face greater risks because many work in vulnerable outdoor occupations like agriculture and construction³⁹. They are 43% more likely to live where rising temperatures may greatly reduce work hours³⁹. Non-Hispanic American Indians/Alaska Natives have the highest heat mortality rate at 0.6 per 100,000 people⁴⁰. Multiple factors contribute to the higher mortality rates from heatwaves among minorities and those with lower socioeconomic status^{41,42}, depicting noticeable regional variations⁴³. These include, for example, lack of access to air conditioning, pre-existing health conditions like cardiovascular disease, use of medications that inhibit thermoregulation, and residence in urban heat islands with higher temperatures^{40,42}. For instance, the impacts are especially widespread and dangerous in the Southern states, where global warming is expected to bring up to 70 consecutive days annually with heat indices above 38 °C in states like Texas and Florida⁴³. Designing sustainable strategies to manage the risk of rising temperature requires sound understanding of spatiotemporal characteristics of heatwaves at decision relevant scales^{16,24,44}.

Several previous studies provide important insights on spatio-temporal characterizations of heatwaves and their socioeconomic impacts on a larger scale. For example, studies^{5,10,36} highlighted the substantial heatwave burden on health and social systems, threatening ecological diversity worldwide. The Intergovernmental Panel on Climate Change^{18,45} analyzed heatwave trends across the USA and discussed how deadly heatwaves are overheat tolerance limits. However, some key limitations remain in terms of location-specific (such as, at county level) multivariate heatwave characterization and integrated analysis with social vulnerability. Many studies^{5,29,46–49} have focused on understanding impacts of heatwaves across regional to global scales by analyzing their characteristics, particularly focusing on daytime extremes with limited characterization of physical and sociodemographic attributes. We expand on previous studies by (i) focusing on a historically vulnerable communities, (ii) characterizing spatiotemporal variation of heatwave at county level, (iii) leveraging high-resolution reanalysis dataset, (iv) analyzing multiple heatwave characteristics, (v) providing comprehensive analysis of nighttime, day–night, and combined temperatures, and (vi) developing decision-relevant metrics to account for diverse physical and sociodemographic attributes.

The key objective of this study is to assess spatiotemporal characterization of heatwave exposure across historically vulnerable communities. We provide a comprehensive characterization of heatwave implications, trends, effects, and develop an integrated risk index. We integrate multiple heatwave indicators (including frequency, duration, and magnitude) and datasets (daytime, nighttime, average, and throughout the day to night), and overlay the quantified heatwave hazards with a social vulnerability index to identify regions facing compounded risks from physical heat exposure and socioeconomic sensitivity. This can enhance community resilience to extreme heat events.

Study area

Mississippi is chosen as our research focal point due to its unique characteristics that make it an ideal location for investigating heat wave effects, particularly in relation to social vulnerability. Climate change has the disproportionate impact of heat stress on regions like Mississippi⁵⁰. Extreme heat is projected to cost the USA half a trillion dollars annually by 2050, with Mississippi, Texas, and Alabama experiencing some of the highest economic losses and potential future increases²². Mississippi's susceptibility to heatwaves is influenced by its climatic characteristics^{51,52}, making it an essential region for understanding the multifaceted consequences of extreme heat events. Additionally, the state possesses a diverse socio-economic landscape, which offers an excellent opportunity to explore how heatwave hazard can affect various demographic groups and economic conditions, as depicted in Fig. 1B. We can see that Mississippi has the lowest per capita personal income compared to other states in the United States⁵³ (Fig. 1A). The region has around 25% of its total population under 5 years old or over 65, the age groups most vulnerable to heatwaves, the age groups most vulnerable to heatwaves, as shown in Fig. 1C⁵⁴. Furthermore, there is a significant relevance in addressing urgent climate change and public health issues, given its vulnerability to extreme heat and its socioeconomic diversities.

Data and methodology

Data collection

This study utilizes two separate datasets to compute heatwave indices, and a third dataset for generating the social vulnerability index and humidity dataset to calculate heat index. The first dataset comprises ground-based weather station data (hereinafter reference observations). The Meteostat Python library⁵⁶ is used for this purpose. A total of 39 weather stations is identified across the Mississippi with long-term hourly temperature data spanning from 1980 to 2022. However, after careful evaluation, only six stations have data available for the entire specific period (1982–2022). Among these six stations, two have data gaps from December 1999 to January 2005, making them unsuitable for our analysis. We ultimately utilize data from the remaining four weather stations that

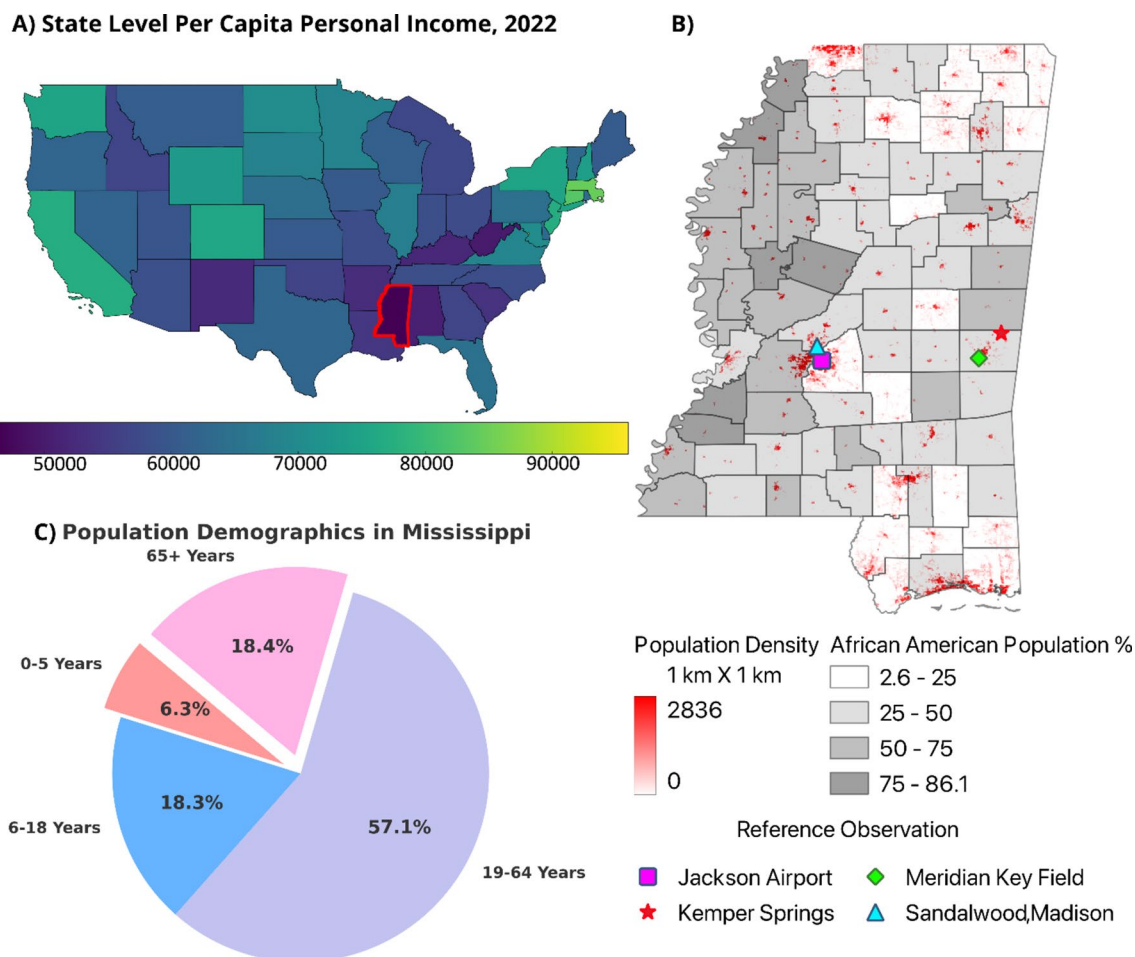


Fig. 1. Spatial distribution of county-level (A) per capita income by state for 2022, showing Mississippi in red, and (B) distribution of African American population percentage in Mississippi, with color gradient from black indicating higher percentages to white indicating lower. Red spots signify population density per 1 km × 1 km grid. The four points represent reference ground stations to check accuracy of ERA5 reanalysis data (a global atmospheric reanalysis dataset produced by the European Center for Medium-Range Weather Forecasts)⁵⁵. (C) Pie Chart showing distribution by age groups for Mississippi.

consistently recorded temperature data between 1980 and 2022. The four weather stations details are presented in Table 1 and shown in Fig. 1B. These stations are gone through detailed analysis. Additionally, data from the other stations (those with shorter time frames or partial data availability, other than the four long-term stations) were considered for a more generic, simpler analysis. These other datasets were used to calculate R2 and RMSE with second dataset (explained next paragraph) to evaluate its suitability for further research. These additional datasets still serve as reference points. The details of those stations are provided in Table S2.

The second dataset used in this study is the ERA5 at hourly scale and 11 km spatial resolution⁵⁵. It is derived from the European Centre for Medium-Range Weather Forecasts, incorporating both model and global observations. The rationale for using ERA5 data lies in its comprehensive coverage, high spatial and temporal resolution, and its proven accuracy in temperature predictions. Studies have shown that ERA5 data is highly accurate for temperature predictions and provides valuable insights into climate research^{57–60}. We extracted the temperature at 2 m above the ground from ERA5. We acquire ERA5 data for the same reference observation stations (N = 39),

| S. N | Weather station | Station ID | Latitude | Longitude |
|------|---------------------|------------|----------|-----------|
| 1 | Meridian key field | 72234 | 32.34N | 88.75W |
| 2 | Kemper springs | KNMM0 | 32.55N | 88.56W |
| 3 | Jackson airport | 72235 | 32.32N | 90.08W |
| 4 | Sandalwood, Madison | KMCBO | 32.44N | 90.12W |

Table 1. List of stations and their locations that are used to test the accuracy and consistency of ERA5 data.

to assess the accuracy of ERA5 data. To evaluate the performance of the ERA5 data, we compute the root mean square error (RMSE) and coefficient of determination (R^2). We aggregate grid data into county-averaged time series data to perform spatial analyses at the county level.

The third dataset that this study employed is the Centers for Disease Control and Prevention/Agency for Toxic Substances and Disease Registry (CDC/ATSDR) Social Vulnerability Index (SVI)⁵⁶ to integrate heatwave exposure with socioeconomic vulnerability. SVI is an advanced geospatial tool developed by the ATSDR to quantify social vulnerability across the Census tracts – statistical subdivisions of counties. This multidimensional index captures vulnerability across four key themes: socioeconomic status, household characteristics, racial and ethnic minority status, and housing type and transportation. Using multidimensional index ensures we do not overlook indirect but important factors that could elevate heat-related hazards and contribute to a community's overall resilience. While the SVI provides a comprehensive approach, other metrics have been developed specifically for assessing heat vulnerability. The Heat Vulnerability Index (HVI)^{61,62}, combines factors such as exposure to extreme heat, sensitivity (e.g., age, health conditions), and adaptive capacity (e.g., access to air conditioning, socioeconomic status). Additionally, studies have highlighted factors like elderly age, childhood, gender, cardiorespiratory diseases, diabetes, and low socioeconomic status as significant contributors to heatwave-related morbidity and hospitalizations⁶³. The SVI offers an advantage by integrating these sensitivity parameters, along with socioeconomic factors, into a single index at the county scale, aligning with our research objectives. This index is formulated using 16 demographic and socioeconomic variables. The detailed description of variables can be found in CDC/ATSDR portal⁶⁴. It allows us to account for the intersectionality of various socioeconomic factors known to influence a community's ability to prepare for, respond to, and recover from environmental hazards like heatwaves.

The fourth dataset used is the University of Idaho Gridded Surface Meteorological Dataset (GRIDMET)⁶⁵, acquired from Google Earth Engine. We extracted the daily maximum relative humidity (rmax) data from GRIDMET at 4.6 km spatial resolution, spanning 1980 to present. GRIDMET integrates surface meteorological observations with topographic data using sophisticated interpolation methods to produce high-resolution gridded estimates of meteorological variables across the conterminous United States. Figure 2 describes the overall methodological framework implemented in this study, and detailed methodology is described in the subsequent sections.

Evaluation of ERA5 data

While ERA5 is generally reliable due to its incorporation of observational data, it also relies on satellite and remote sensing data alongside model outputs. Therefore, assessing the accuracy of ERA5 in our specific context is essential. To assess the reliability/accuracy of ERA5 hourly data, we evaluate its performance with all the reference observations in terms of RMSE and R^2 . We generate violin plots to visually compare the distribution and summary statistics of ERA5 and reference observations. These plots show data distribution, with inner box plots indicating the interquartile range and median. This dual representation facilitates the assessment of distribution similarities and differences between the two datasets. Wider violins and greater median separation indicate larger discrepancies between ERA5 and reference observations. Subsequently, we create hexbin plots to provide a bivariate visualization of ERA5 versus reference observations. These plots divide data points into hexagonal bins, with color intensity reflecting the number of data points in each hexagon. Lower RMSE and higher R^2 values indicate stronger agreement between ERA5 and reference observations. Both these statistical metrics and intuitive visualizations aid to a comprehensive evaluation of the quality and biases in the ERA5 reanalysis and reference observations.

Heatwave indices and their trend

We utilize hourly ERA5 data at the county level to extract daily maximum temperature (T_{max} , representing day) and daily minimum temperature (T_{min} , representing night). Furthermore, we compute the daily average temperature (T_{avg} , representing average) by averaging the hourly data for each day. We also incorporate both daily minimum (Night) and daily maximum (Day) temperatures to gain insights into heatwaves throughout the entire day (i.e., from day to night). In our study, we define a heatwave as a continuous period of three or more days during which the temperature exceeded 95% of the overall temperature data for the respective county (Table 2).

We examine five major characteristics of heat waves for each dataset (Day; Night; Day and Night; Average). In total, 20 heatwave indices (4×5) are used in this study. Heatwave Number (HWN) informs the count of heatwave events that met the criteria of lasting three or more consecutive days. Heatwave Total Days (HWTDD) represents the total count of days that contributed to heatwaves. These are the days during which elevated temperatures met the heatwave criteria. Heatwave Longest Duration (HWLD) measures the length of the longest continuous heatwave event identified by HWN. It identifies the most extended period during which temperatures remain consistently elevated. Heatwave Mean Temperature (HWMT) is simply the average temperature of the heatwaves. Hottest Day Temperature (HDT) focuses on the peak daily temperature within the most intense heatwave event, providing insight into the highest temperature extremes experienced during heatwaves.

We then aggregate heatwave indices on a yearly scale for each county, providing valuable information on the spatiotemporal variations across Mississippi. For this, we compute the long-term average value of each heatwave index to gain insights into spatial heterogeneity. And to assess temporal trends, we then compute the Sen's slope⁶⁶ of each heatwave index for each county, in conjunction with a non-parametric Mann–Kendall test^{67,68}. For trend detection, we employ a python package `pyMannKendall` using an original Mann–Kendall test⁶⁹. The original Mann–Kendall test is a nonparametric test, which does not consider serial correlation or seasonal effects⁶⁹. The Mann–Kendall p-value indicates the level of statistical significance associated with the trend. We consider a p-value of 0.1 (or 90% confidence) to denote statistical significance. In simpler terms, a

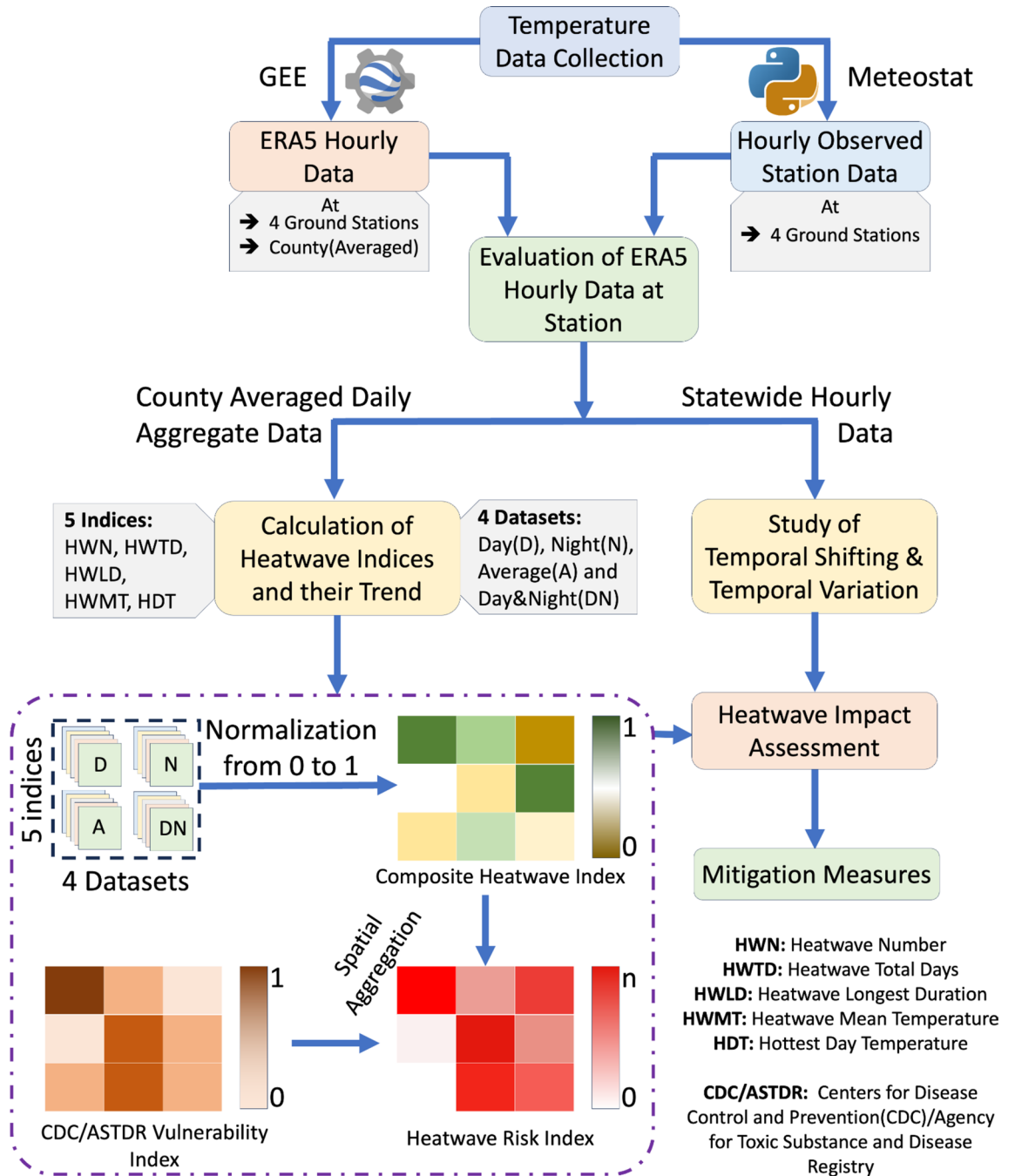


Fig. 2. Schematic diagram of the overall methodology adopted in this study.

| Dataset | Heatwave condition | Minimum duration |
|---------------|---|--------------------|
| Day | $T_{max} > T_{max_{95}}$ | 3 consecutive days |
| Night | $T_{min} > T_{min_{95}}$ | 3 consecutive days |
| Day and night | $T_{max} > T_{max_{95}}$ and $T_{min} > T_{min_{95}}$ | 3 consecutive days |
| Average | $T_{avg} > T_{avg_{95}}$ | 3 consecutive days |

Table 2. Definition of heatwave based on the percentile for different datasets. T_{max} , T_{min} and T_{avg} are the daily maximum, daily minimum and average of daily maximum and minimum temperatures, respectively. The subscript 95th means the 95th percentile.

p-value below 0.10 suggests a less than 10% probability that the trend occurred randomly⁶⁹. By combining the linear slope with the Mann–Kendall p-value, we quantify the direction, magnitude, and significance of heatwave trends at the county level.

Evaluation of temporal shifting

To assess potential changes in the seasonal timing and inter annual variation, we aggregate the ERA5 temperature (Tmax, Tmin and Tavg) into monthly averages for each of the 82 counties in Mississippi. Monthly Tmax informs temporal shifts in the hottest summer daytime temperatures over the year. Similarly, monthly Tmin describes changes in nighttime temperatures, as minimum temperatures typically occur overnight. Meanwhile, the monthly Tavg provides insights into shifts in the overall temperature cycle (if any).

Superimposition with socioeconomic parameters

We finally have a composite heatwave index to represent the overall intensity of heatwave at the county level. All heatwave indices (HWN, HWTD, HWLD, HWMT, and HDT) computed for day, night, day–night, and average temperature datasets (resulting in 20 heatwave indices) are initially normalized to a 0–1 scale individually, using the MinMaxScaler from the scikit-learn Python package⁷⁰. These normalized indices are then averaged arithmetically to generate a comprehensive composite heatwave index. This composite index integrates the multi-dimensional aspects of heatwave intensity, frequency, duration, and magnitude into a unified metric. The rationale for this comprehensive approach is to capture all relevant dimensions of heatwaves and to account for the variations between the indices ensuring the composite index accurately reflects overall heat stress. Additionally, it allows for a concise visualization of the spatial patterns of heatwave hazards across counties, enabling overlay with socioeconomic vulnerabilities. Mapping this comprehensive heatwave index reveals county-level hot and cold spots of heat hazards and exposure. For superimposing the composite heatwave index with the composite SVI, we employed a ranking-based approach. Both the composite heatwave index and the SVI were divided into 100 percentiles. Each county was assigned a rank from 1 to 100 for both the composite heatwave index and the SVI, reflecting their respective positions within the distribution. These ranks were then summed to produce a Combined Vulnerability Score for each county. This method ensures that extremes in either index (heatwave or socioeconomic vulnerability) are effectively captured in the combined score, rather than being averaged out. Finally, the Combined Vulnerability Score was normalized to a 0–1 scale using the MinMaxScaler, resulting in the Heatwave Risk Index (HWRI). The HWRI thus integrates both physical heat exposure and population sensitivity aspects into a unified metric. This final integrated metric reveals counties with the highest combined risks from heatwaves and vulnerability. The proposed HWRI offers a replicable framework for comprehensive spatiotemporal analysis, evaluating heat extremes through a multidimensional lens.

Heat index: temperature and humidity

The heat index is a measure of how hot the ambient air feels to the human body when relative humidity is combined with the air temperature. It is an important metric for assessing human discomfort and the potential for heat-related illnesses. We calculated the heat index for our study region using the equations developed by Rothfus (1990) and adopted by the National Weather Service (NWS)^{71–73}. The heat index (HI) is computed for two scenarios (i) Average HI for the entire study period (1982–2022) and (ii) Average HI for days when heatwave conditions occurred.

The heat index (HI) is computed as follows:

1. A simple formula was applied first:

$$HI = 0.5\{T + 61.0 + [(T - 68.0)1.2] + (RH0.094)\}$$

2. If HI $\geq 80^\circ\text{F}$, the full regression equation was used with adjustments for certain humidity ranges:

$$HI = -42.379 + 2.04901523T + 10.14333127 \times RH \\ - 0.22475541 \times T \times RH - 0.00683783 \times T^2 - 0.05481717 \times RH^2 + 0.00122874 \times T^2 \times RH \\ + 0.00085282 \times T \times RH^2 - 0.00000199 \times T^2 \times RH^2$$

Adjustments:

- If RH < 13% and $80^\circ\text{F} \leq T \leq 112^\circ\text{F}$:

$$\text{Adjustment} = \frac{13 - RH}{4} \times \sqrt{\frac{17 - |T - 95|}{17}}$$

$$HI = HI - \text{Adjustment}$$

- If RH > 85% and $80^\circ\text{F} \leq T \leq 87^\circ\text{F}$:

$$\text{Adjustment} = \frac{RH - 85}{10} \times \frac{87 - T}{5}$$

$$HI = HI + \text{Adjustment}$$

where T is maximum temperature ($^\circ\text{F}$) and RH is relative humidity captured from (%).

We implement this heat index calculation in Python. After obtaining the heat index values, we visualized their spatiotemporal patterns across Mississippi counties to characterize human discomfort during heatwave events.

Results

Evaluation of ERA5 data

Figure 3 shows a comparison between ERA5 and four best reference observations. The medians, quartiles, and other statistical characteristics for both ERA5 and reference observations at all four stations are closely aligned (First row Fig. 3). This alignment indicates that ERA5 data closely mimicked the reference observations. Additionally, the shape of the violins and the proximity of the medians suggest a strong similarity in the distribution of temperature data between ERA5 and reference observations.

In the second row of Fig. 3, hexbin plots offer a spatial visualization of the ERA5 versus reference observations. The pronounced diagonal alignment illustrates a very strong correlation, with the highest densities centered along the 1:1 line ($R^2 > 0.94$). Additionally, lower RMSE values (from 1.77 to 2.17) demonstrate the small magnitude of differences between ERA5 and reference observations. These high R^2 values and lower RMSE values reinforce the notion that ERA5 closely approximates the reference observations. Furthermore, the consistent availability of ERA5 data across the space enhances its applicability, even in areas where ground-level data may be scarce or unavailable.

Additionally, an evaluation conducted for other stations with partial or shorter time frames of data, is detailed in Table S1. These stations, located throughout various parts of Mississippi (Figure S1), demonstrate R^2 values greater than 0.94 and RMSE values less than 2.5 for 34 out of 37 stations. This high level of agreement is depicted in Figure S1A and B. The robust performance across these additional stations further confirms the reliability of ERA5 data for the analysis across the region.

Social vulnerability index

Our analysis of county-level SVI data of Mississippi reveals a patchwork of place-based fragilities requiring targeted policy interventions. 40 of 82 counties exhibit above-average socioeconomic vulnerabilities, with the index exceeding 0.5 (where 0 and 1 denote lowest and highest vulnerability respectively). There are sharp contrasts in vulnerability within the state (Fig. 4B). The poorer northwest Delta area faces more widespread challenges like high poverty and poor job access compared to more resilient southern counties (SVI average ~ 0.35). Similarly, household vulnerability greatly differs between the highly fragile centrally located counties (Scott County) and minimally fragile Lafayette County, pointing to clear spatial inequality in resilience across sub-state areas (Fig. 4C).

Overlaying spatial and socioeconomic analyses provides an overview of vulnerability (Fig. 4D). We find Holmes County encounters the highest composite SVI, followed by Washington and Noxubee—all located in the northwest (Fig. 4D). It suggests resilience deficits are modulated by intersectional education, health, and racial inequities, predominantly in the African American Delta sub-region. Meanwhile, 41 counties statewide show above-average cumulative vulnerability indices, pointing to diverse yet sporadic fragilities necessitating comprehensive, context-specific interventions.

Our integrated spatial-demographic analysis reveals that larger populations (Fig. 4A) do not preclude high social vulnerability (Fig. 4B). Washington County (The locations of each county and its corresponding county ID number can be found in Supplementary Figure S5 and Table S2), with the 6th highest population statewide

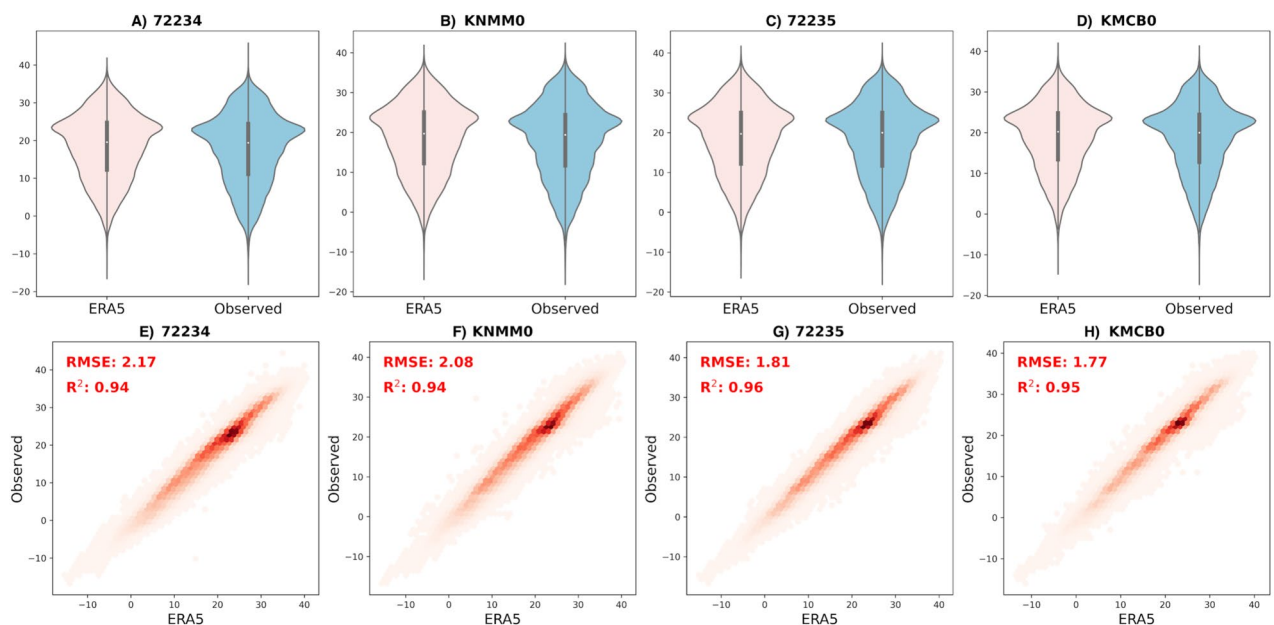


Fig. 3. Comparison of ERA5 and ground-level temperature data for four Mississippi stations: Meridian Key Field (Station ID: 72234), Meridian/Kemper Springs (Station ID: KNMM0), Jackson Airport (Station ID: 72235), and Madison/Sandalwood (Station ID: KMCB0). The first row (3 A–D) shows violin plot distributions and the second row (3 E–H) presents hexbin scatter plots with RMSE and R^2 values in red.

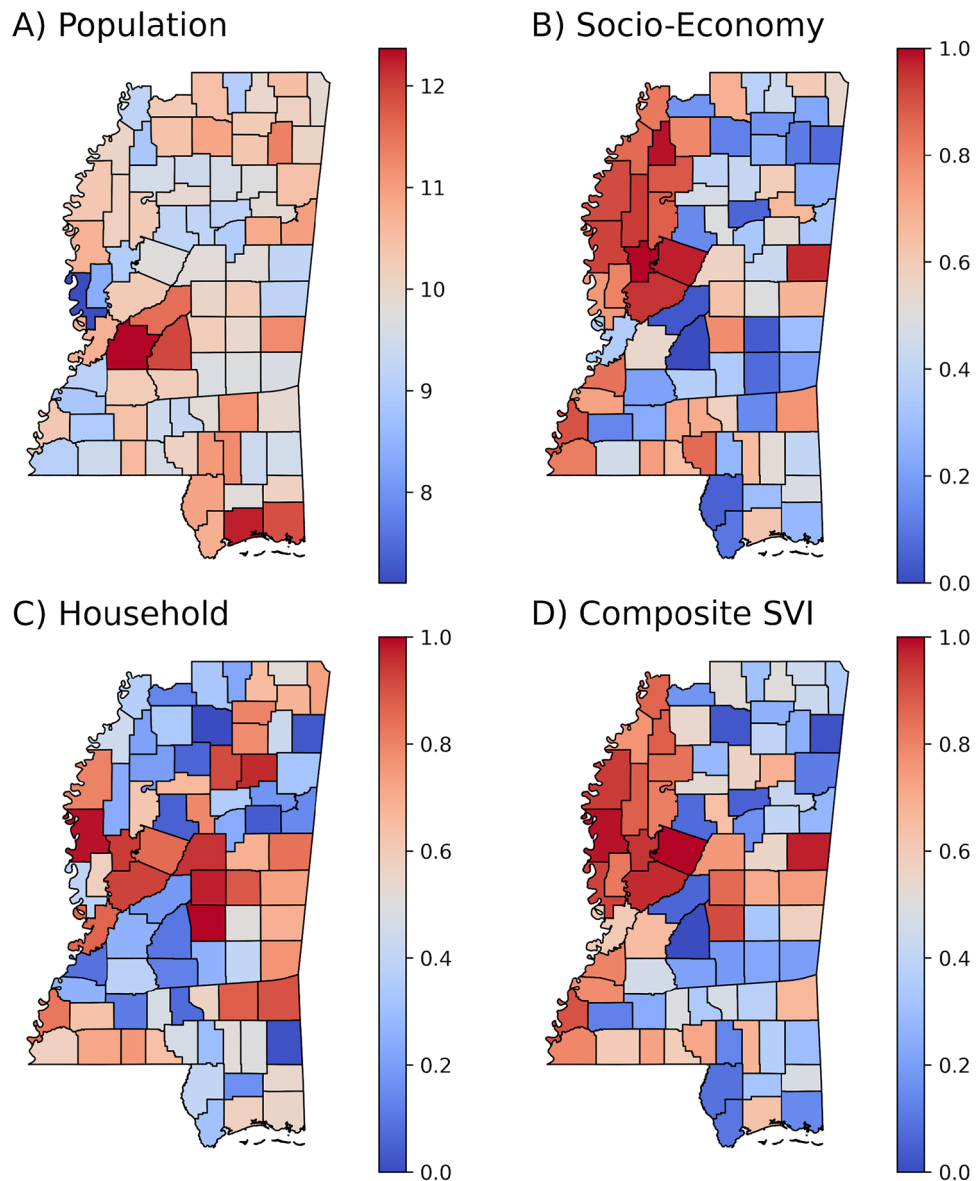


Fig. 4. Spatial distribution of county-level: (A) Population in logarithmic scale, (B) Socioeconomic Status Index, (C) Household Characteristics Index, and (D) Composite Social Vulnerability Index (SVI).

(44,604 residents), displays near-maximum vulnerability (SVI - 0.9877). Comparably populous Hinds County (226,541 residents) exhibits moderate vulnerability (SVI - 0.6543), likely cushioned by urban resources. However, rural Yazoo County faces disproportionately high vulnerability (SVI - 0.9630) despite having under 30,000 residents. Also, Figure S6 shows the ratio of vulnerable population to the total population for every county is similar. These highly variable associations underscore that population size alone does not accurately predict resilience or precarity, yet tracking demographics enriches this multidimensional metric and can guide interventions prioritizing dignity for marginalized communities.

Heatwave indices and their trend

The spatial distribution of the mean heatwave number (HWN) over the study period reveals distinct daytime versus nighttime patterns (Fig. 5A and B). The distribution of daytime HWN indicates that the northeastern and coastal counties stand out as relatively hotspots. Only coastal counties emerge as prone to frequent nighttime heatwaves (Fig. 5A), as minimum temperatures consistently remain elevated because of high specific heat capacity of water. The average temperature HWN plot combines these effects, with hotspots in northern and coastal regions (Fig. 5C). The western counties exhibit only slightly lower HWN, with the range being approximately 2.0–2.5 days, suggesting a relatively uniform frequency of heatwaves.

Critically, the day–night combined HWN (Fig. 5D) shows widespread extreme values across Mississippi. The minimal spatial variation indicates that most counties experience similar heatwaves persisting both day

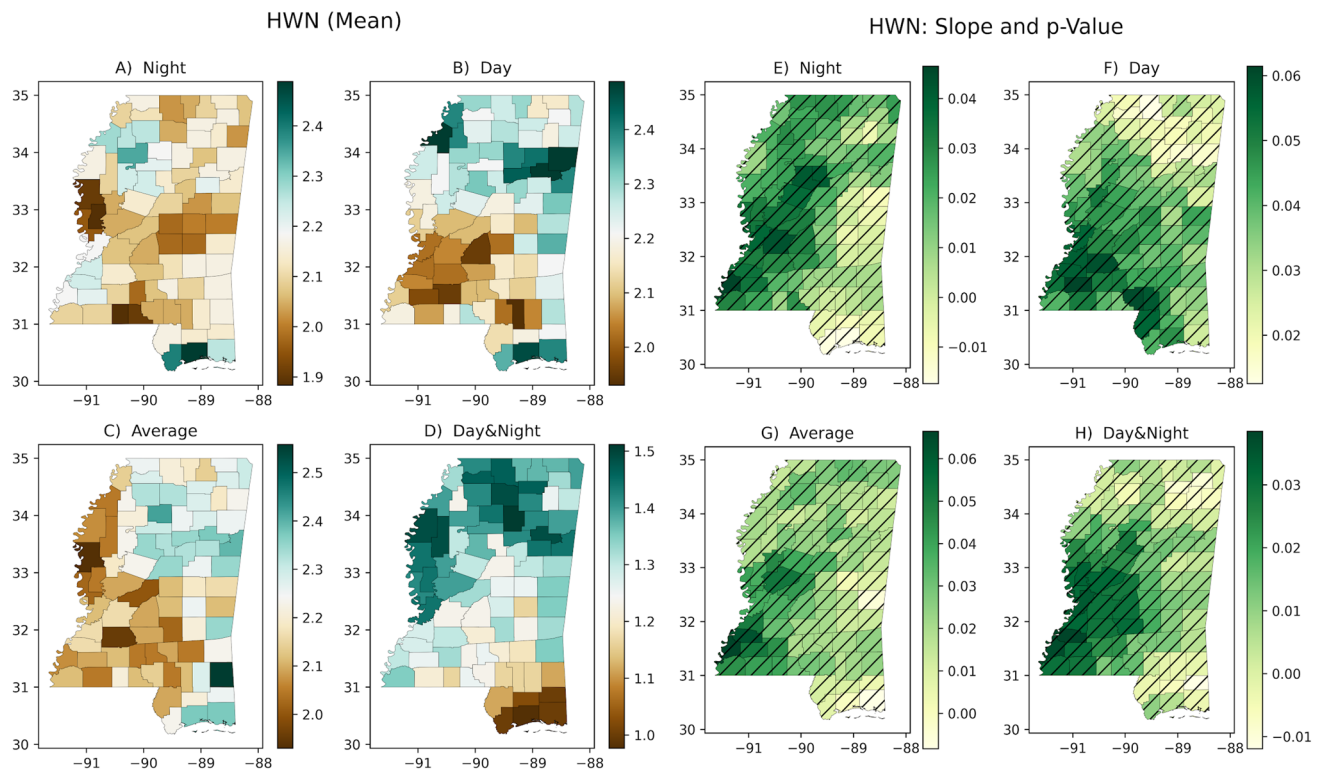


Fig. 5. County-level spatial distribution and temporal trends of heatwave number (HWN). (A–D) Maps showing mean values of HWN during the study period from 1980 to 2022 for day, night, day–night combined, and average temperature datasets. (E–H) Maps visualizing linear temporal trends in HWN. Hashed counties represent significant slopes at 90% confidence level.

and night. Persistent exposure through day to night creates substantial health and infrastructure risks⁷⁴, that are prevalent for most counties statewide. Moreover, positive HWN slopes are widespread (Fig. 5E–H), indicating an increasing frequency of heatwaves during the day, night, and especially in the combined day–night periods. Notably, counties with fewer heatwaves exhibit steeper and highly significant positive trends. Meaning, these regions with even lower heatwave events in the past are likely to accelerate. Importantly, rising trends across existing hotspots are crucial.

The spatial patterns and trends in HWTD are shown in Fig. 6. HWTD represents the cumulative count of days contributing to heatwaves annually. The mean annual values of HWTD (Fig. 6A–D) reveals relatively uniform exposure of 12–14 days statewide for the daytime dataset. Slightly lower nighttime HWTD of 11–13 days indicates marginal overnight relief. The average temperature HWTD combines these day–night cycles. Critically, the day–night combined HWTD exhibits pervasive extremes of ~7 days annually, representing persistent multi-day heatwaves. For vulnerable groups, this constant exposure without nighttime respite could severely threaten health⁷⁴. Northern and western counties experience slightly more day–night heatwave days.

Day and nighttime HWTD slopes exhibit a rising trend, demonstrating intensification of heatwave days over time. For the critical day–night combined HWTD, noticeable negative slopes can be found along the coast and northeast. These declining trends are also statistically significant indicating these counties may experience some relief from prolonged heatwaves, though overall HWNs are still increasing. It implies that although the total HWTDs will decrease, there are likely chances of recurrent heatwaves but of shorter durations. Also looking at HWLD (Figure S2), the persistent heatwave duration of 4–8 days and its statistically significant rise underscores the likely risk for consecutive days to people, livelihood, and environment^{6,75}. Continued increases in parts of the southwest could exacerbate threats to health, agriculture, and infrastructure during the most extreme heatwave events each year⁷⁶.

HWMT represents the average temperature across all days comprising heatwaves each year. Figure 7A–D show the spatial distribution of mean HWMT from 1980 to 2022. Daytime heatwaves reach summertime highs around 28–29 °C on average statewide, with slightly cooler northeastern counties. At night, coastal regions experience elevated minimum HWMT near 23 °C due to moderating Gulf breezes. The day–night combined HWMT exhibits pervasive extremes exceeding 20 °C at average across Mississippi. Regarding trends (Fig. 7E–H), no statistically significant changes are observed for any dataset. While some counties show moderately positive or negative slope magnitudes, the patterns are scattered with no spatial coherence. The mean heatwave temperature appears to be increasing but there is no statistical significance. Extremely high heatwave temperatures above 35 °C, which can overwhelm the body's ability to cool itself even with fans⁷⁴, remain a major concern. Such extreme heat can impact critical infrastructure systems like energy, transport, water, and healthcare services^{77,78}, potentially causing blackouts, transport disruptions, water shortages, and reduced hospital capacity. Heat waves also pose significant health risks, especially for vulnerable populations like older adults, those with underlying

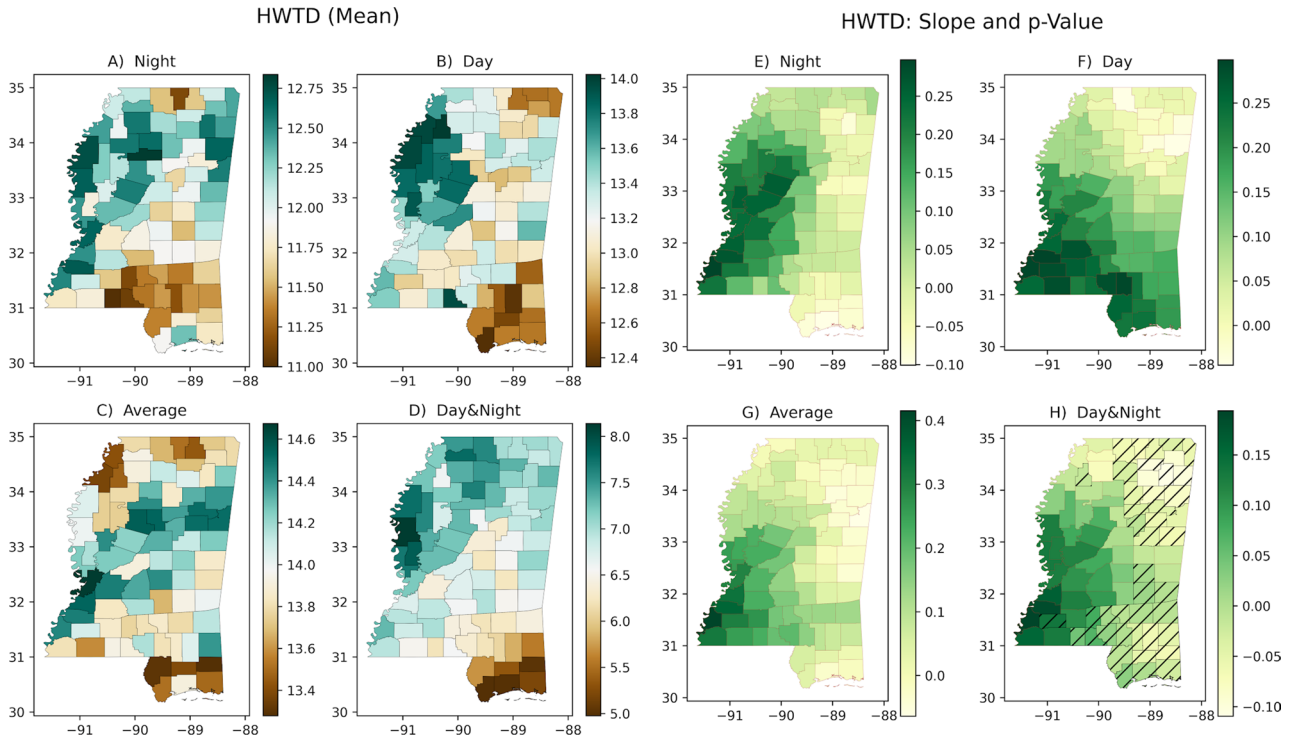


Fig. 6. County-level spatial distribution and temporal trends of heatwave total days (HWTD). (A–D) Maps showing mean values of HWTD during the study period from 1980 to 2022 for day, night, day–night combined, and average temperature datasets. (E–H) Maps visualizing linear temporal trends in HWTD. Hashed counties represent significant slopes at 90% confidence level.

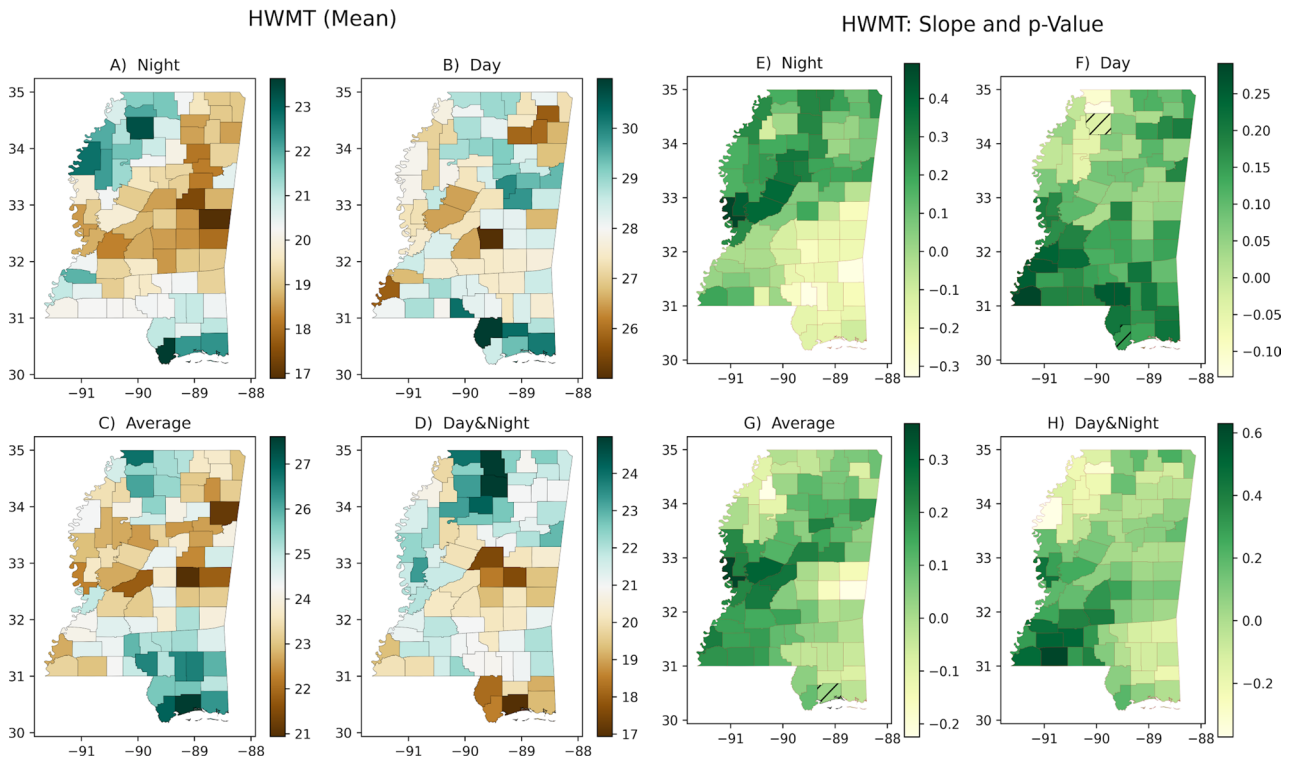


Fig. 7. County-level spatial distribution and temporal trends of heatwave mean temperature (HWMT). (A–D) Maps showing mean values of HWMT during the study period from 1980 to 2022 for day, night, day–night combined, and average temperature datasets. (E–H) Maps visualizing linear temporal trends in HWMT. Hashed counties represent significant slopes at 90% confidence level.

medical conditions such as asthma^{79,80}, and outdoor workers^{81,82}. Monitoring and implementing protective measures against extreme heatwave temperatures is critical to mitigate impacts on infrastructure function and human health and productivity.

Observations confirm that heatwaves are occurring more often and lasting longer across Mississippi. For example, all counties exhibited positive HWN slopes in day and average dataset and 90% of counties in night and day–night dataset, and these trends are statistically significant. Spatial analysis reveals concerning patterns of elevated risk, particularly for persistent day–night heat exposure. Among the datasets, the day–night combined metrics stand out as exhibiting the most pervasive, extreme, and statistically significant upward trends in both number of heatwave events and their durations. This constant heat stress poses severe threats to health⁸¹, as the human body requires cooler overnight temperatures, ideally below 25 °C, to recover from hazardous daytime conditions^{74–76}.

Figure 8 shows the temporal variation of HWN and HWTD. The recent 20 years exhibit markedly higher frequencies of extreme peaks in annual heatwave numbers and total heatwave days compared to the prior two decades. For instance, years after 2000 feature multiple instances of six or more heatwaves and over 35 total heatwave days annually. The year 2010–12 stands out as an exceptional extreme, with seven heatwaves and around 45 heatwave days statewide. While maximum single-event heatwave duration and peak heatwave temperature metrics remained relatively stationary, the uptrends in frequency and total days are the dominant signals. Even if individual heatwaves are not lengthening or reaching hotter extremes, the fact that more heatwaves are occurring and lasting longer creates significant risks.

Evaluation of temporal shifting

The temporal variations of monthly Tmax, Tmin, and Tavg are shown in Figure S4 in the supplementary section. The Tmax heatmap reveals pronounced progression toward more intense extreme heat in May and September in recent years. Isolated dark red colors emerge in October starting in 2019, marking the first instances of extreme heat that late in the season. Even the winter months of January and February display slightly warmer indications in recent decades. This demonstrates that peak summertime heat is steadily advancing earlier in spring and persisting later into fall. Notably, the patterns differ between pre- and post-2000. Notably, 2011 and 2012 exhibit pronounced intensification, with consecutive higher Tmax and Tmin across June through August. This corresponds to higher Tavg, reflecting extreme heat persistence day and night. Also, the year 2000 stands out as an extreme event, spanning July through September. Minimal shifting is observed in winter months, and night heat extremes have remained relatively stationary.

Superimposition with socioeconomic parameters

The spatial pattern of the normalized heatwave composite index is shown in Fig. 9A. Consistent with the individual heatwave metrics analyzed previously, the composite identifies counties across northwest Mississippi as severe hotspots, with values exceeding 0.8. The highest severity is observed in Yalobusha County with 12,364 people⁸³. Bolivar, Lafayette, Panola, and Tallahatchie counties also emerge as extreme heatwave hotspots based on the integrated metric. In total, 25 counties display a composite heatwave index over 0.5, concentrated primarily across the northwest. These regions exhibit consistently high heatwave numbers, durations, and magnitudes

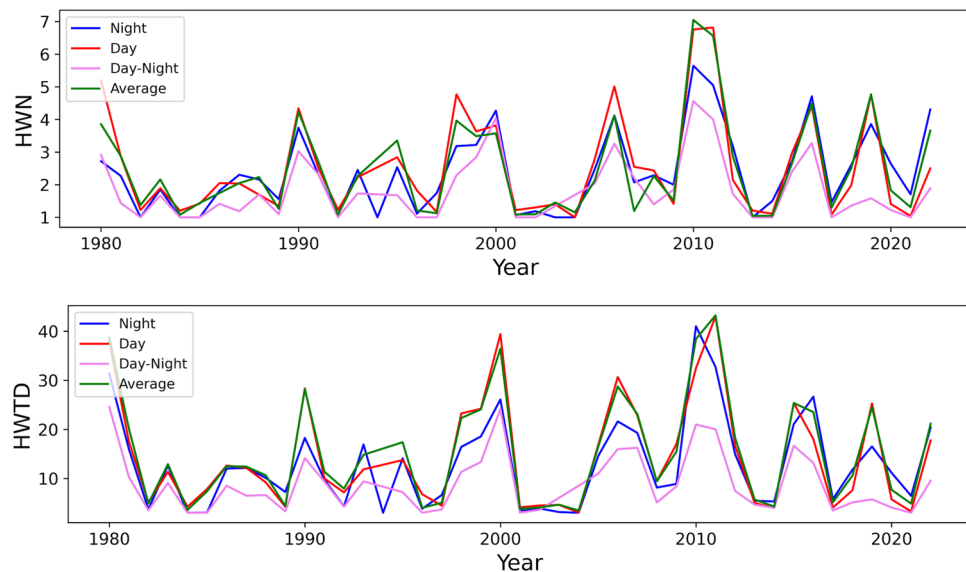


Fig. 8. Inter annual variation of heatwave number (HWN) (top) and annual heatwave total days (HWTD) (bottom) for Mississippi over the period 1980–2022. The last two decades exhibit more frequent extreme peaks in HWN and HWTD compared to 1980–2000, providing further evidence of intensifying heatwaves statewide in recent years.

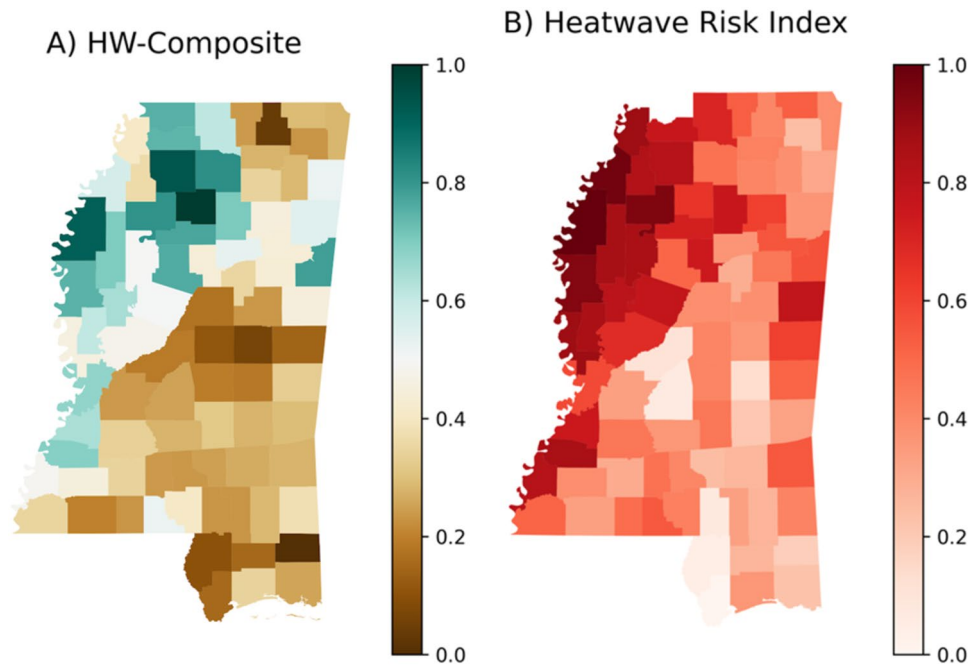


Fig. 9. Spatial distribution of county-level (A) composite heatwave index, and (B) heatwave risk index.

based on the individual metrics. 50 counties exhibit composite values below 0.2, indicative of relatively lower heatwave intensity. The lowest index occurs around coastal regions of Mississippi and George County with 25,206 people living there⁸⁴.

Importantly, as illustrated in Fig. 4D, these northwest counties also exhibit heightened social vulnerability. The HWRI (Fig. 9B) accounts for both physical heat exposure and socioeconomic vulnerability. Consistent with the individual maps, the integrated index shows highest risk levels concentrated across northwest Mississippi. Bolivar county emerges as the top hotspot, with a risk index 1. Tallahatchie, Coahoma and Washington counties follow closely behind with values over 0.9. Overall, 18 counties display risk levels >0.75 and 36 counties display risk levels >0.5, mostly located within the elevated heatwave and vulnerability region in the northwest.

Heat index: temperature and humidity

The county-level analysis of average heat index values across Mississippi reveals substantial spatial variations across the study period (1982–2022) as well as during heatwave events (Fig. 10). For the average study period heat

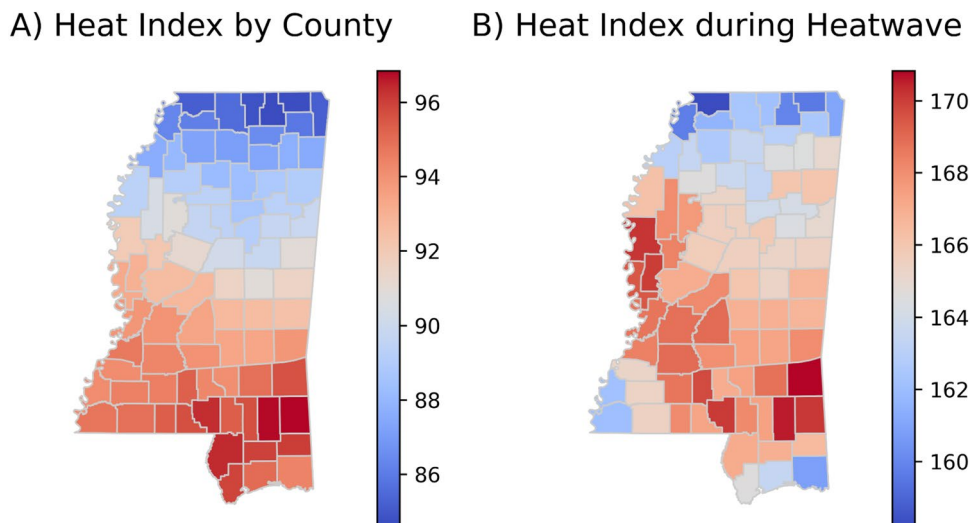


Fig. 10. Spatial distribution of average heat index across Mississippi counties, with a color ramp indicating increasing heat index values from blue (cooler) to red (hotter).

index (Fig. 10A), the southern counties generally experience higher levels compared to the northern counties. The mean heat index for all 82 counties is 92.3°F, with a median of 92.6°F. The values range from a minimum of 84.6°F in Tippah County, classified as "Caution" according to the heat index scale in Figure S7, to a maximum of 96.8°F in Greene County, which falls into the "Extreme Caution" category as per NWS^{73,85}. The top ten counties with the highest average heat index are predominantly located in the southern part of the state: Greene (96.8°F), Perry (96.8°F), Marion (96.3°F), George (96.0°F), Pearl River (96.4°F), Hancock (95.9°F), Stone (96.0°F), Forrest (95.7°F), Walthall (95.7°F), and Lamar (95.3°F) counties. These counties experience oppressively high heat index levels above 95°F on average, posing significant risks for heat-related illnesses and discomfort, as they fall into the "Extreme Caution" or "Danger" categories. In contrast, the counties with the lowest average heat index values are concentrated in the northern regions of Mississippi, primarily in the "Caution" range: Tippah (84.6°F), Alcorn (84.7°F), Benton (84.9°F), Tishomingo (85.2°F), DeSoto (85.2°F), Prentiss (85.9°F), Marshall (85.6°F), and Tate (86.2°F) counties.

However, during heatwave periods (Fig. 10B), the heat index values are significantly elevated across the entire state, reaching dangerous and even life-threatening levels. The mean heat index soars to 166.6°F, with a median of 166.7°F, firmly in the "Extreme Danger" category ($\geq 125^\circ\text{F}$). All the counties experience exceptionally high heat index values exceeding 168°F during heatwaves, well into the "Extreme Danger" range. The top five counties are Wayne (170.8°F), Washington (170.2°F), Greene (170.1°F), Perry (170.6°F), and Marion (170.1°F). Even counties with relatively lower heat index values during heatwaves, such as DeSoto (158.2°F), Alcorn (159.6°F), Tippah (159.9°F), and Tishomingo (161.0°F), still experience dangerously high levels in the "Extreme Danger" category (125°F and higher), posing significant risks for heat stress and discomfort. The spatial pattern during heatwaves (Fig. 10B) highlights the central and southern regions as hotspots, with a continuous band of counties stretching from the southwest to the southeast experiencing the most severe heat index conditions in the "Extreme Danger" range above 168°F.

Discussion

We observe that the distribution of daytime and nighttime heatwave numbers (HWN) at coastal areas is relatively high, as depicted in Fig. 5A and B. A similar pattern emerges for heatwave total duration (HWTDD) in Fig. 6A and B, heatwave longest duration (HWLD) in Figure S2, heatwave maximum temperature (HWMT) in Fig. 7A and B, and heat day threshold (HDT) in Figure S3, suggesting that coastal cities are particularly vulnerable to heatwaves. The higher nighttime heatwave indices in these areas could be attributed to the higher specific heat capacity of water bodies, which can retain and release heat more effectively than land. However, during daytime, the interplay of marine heatwaves and wind direction may contribute to the elevated heatwave indices observed in coastal regions, warranting further investigation into these potential drivers^{86,87}.

Notably, Fig. 5G reveals a significant increase in the slope of heatwave number with other indices at both daytime and nighttime across all counties, a pattern that is consistently observed in Figs. 6, 7, 8 and S1–S2 for other heatwave metrics. This finding is particularly concerning, as continuous heatwave exposure during both day and night can have severe implications for human health and well-being. While daytime heatwaves necessitate rest and recovery, the lack of respite during the night can prevent the body from recuperating effectively. Constant exposure to heatwaves without a break can pose significant health threats, as supported by numerous studies^{6,75}. Furthermore, the persistent heatwave longest duration (HWLD) of 4–8 days and its statistically significant rise, as shown in Figure S2, underscores the likely risk for consecutive days of heatwave exposure to people, livelihoods, and the environment. Continued increases in parts of the southwest could exacerbate threats to health, agriculture, and infrastructure during the most extreme heatwave events each year^{6,75,76}. Extremely high heatwave temperatures above 35 °C during the daytime as seen in Figs. 7 and S2, which can overwhelm the body's ability to cool itself even with fans, remain a major concern. Such extreme heat can impact critical infrastructure systems like energy, transport, water, and healthcare services, potentially causing blackouts, transport disruptions, water shortages, and reduced hospital capacity^{77,78,82,88}. Of particular concern are the extreme heat index values observed during heatwave periods across Mississippi (Fig. 10B). The mean heat index (which is apparent temperature) soars to 166.6°F, with multiple counties exceeding 168°F, approaching life-threatening levels. The highest value of 170.8°F during heatwaves in Wayne County poses severe health risks, especially for vulnerable populations like the elderly, young children, and those with pre-existing medical conditions. Apart from that, having a heat index above 90°F in half of the counties on an average means they are at extreme caution which could create heat stroke, heat cramps, or heat exhaustion with prolonged exposure as suggested by NWS HI table^{73,85} (Figure S7). When we consider the socioeconomic factors, as illustrated in Fig. 9A and B, it becomes evident that areas with lower socioeconomic conditions tend to have higher heatwave exposure. These communities may lack access to air conditioning or other cooling facilities, exacerbating the impact of heatwaves on vulnerable populations and highlighting the need for targeted interventions and support systems as per the data from CDC/ASTDR⁶⁴. Monitoring and implementing protective measures against extreme heatwave temperatures are critical to mitigate impacts on infrastructure function and human health and productivity.

Most importantly, this focal area faces disproportionate heatwave impacts due to the compounding effects of extreme heat and social disadvantage. There is a clear connection between the data shown in Figs. 2B, 4D, 9A and B. Figure 2B shows that the northwest counties of Mississippi have a significant African American population. These same counties are depicted in Fig. 4D as having high social vulnerability. Figure 9B displays the heatwave risk index, which shows that the northwest counties with more African Americans and higher social vulnerability also experience greater impacts. So even though these counties have lower overall populations as seen in 2B, the minority populations there are disproportionately affected by heatwaves, both socially and physically. This data highlights the need for targeted mitigation measures in these communities to reduce the outsized risks from heatwaves. With events becoming more frequent and prolonged, pressure on public health, agriculture,

infrastructure, emergency response, and social support systems will continue growing. Urgent, proactive intervention through heat resilience plans, warning systems, community preparedness, and infrastructure adaptations are essential to mitigate the likely escalation in extreme heat.

Our findings have significant practical implications that necessitate action from both residents in impacted areas and management departments. For residents, especially in high-risk northwest counties with minority populations and higher social vulnerability, raising awareness through heat action plans, guidelines for staying hydrated and cool, and recognizing heat-related illness symptoms are crucial. Management departments should prioritize interventions and resource allocation in these vulnerable areas, including implementing targeted public health campaigns, expanding access to cooling centers and air-conditioned public spaces, improving emergency response systems, and integrating heat mitigation strategies into urban design and infrastructure development. Importantly, this study highlights the need for long-term, systemic changes to address the root causes of social vulnerability and environmental injustice that exacerbate the disproportionate impact of heatwaves on disadvantaged communities. Collaborative efforts between local governments, community organizations, and stakeholders are essential to develop comprehensive heat resilience plans that tackle socioeconomic disparities, improve access to healthcare and social services, and promote sustainable urban development.

The multifaceted characterization of escalating heatwave regimes and associated vulnerabilities in this study provides a pivotal basis for life-saving interventions. The spatiotemporal patterns of heatwaves, including the extreme heat index values observed during events, emphasize the urgency of local climate action to protect at-risk populations, particularly in already disadvantaged areas facing disproportionate burdens. The integrated Heatwave Risk Index (HWRI) offers a replicable tool to guide equitable decision-making as communities worldwide confront rising extreme heat challenges. The methodological framework developed in this research is scalable and flexible, enabling the heatwave characterization and risk index approaches to be applied to broader regions beyond Mississippi. This provides decision-relevant climate change analysis at local levels worldwide, laying a strong foundation for evidence-based heat mitigation policies centered on social equity. Adaptation efforts prioritizing the identified high-risk counties could significantly enhance community resilience, spotlighting the need to implement timely heat resilience plans across vulnerable areas.

While this study offers valuable insights, it is important to acknowledge limitations and opportunities for further refinement. The heatwave index calculations along with heat index integrating temperature and humidity, provide a crucial measure of human discomfort and heat stress. However, other meteorological factors, such as wind speed and direction, could potentially influence perceived heat exposure and should be considered in future analyses. Incorporating wind patterns, particularly in coastal regions, may shed light on the drivers behind elevated heat indices and enable more targeted mitigation strategies. Furthermore, exploring the interplay between heatwaves and other meteorological phenomena, such as droughts or precipitation patterns, could provide a more comprehensive understanding of the complex interactions shaping heat exposure and its impacts on various sectors, including agriculture, water resources, and ecosystem dynamics. Future research could integrate these additional meteorological variables, along with other relevant factors like land cover, urban heat island effects, and anthropogenic heat sources, to develop more sophisticated heat index models and risk assessment frameworks.

In the subsequent phase, our research aims to investigate local heatwave effects and the potential of nature-based solutions like green and blue infrastructures for mitigating urban heat islands. By combining these findings with localized assessments, we strive to offer actionable recommendations for creating more sustainable and livable cities that are resilient to the increasing challenges posed by heatwaves and climate-related hazards. Overall, proactive measures to avert preventable heatwave impacts will only grow more critical as global warming accelerates. The findings from this study provide a strong foundation for evidence-based policymaking and targeted interventions to enhance heat resilience, particularly in socially vulnerable communities disproportionately affected by extreme heat events.

Conclusion

This study conducted a comprehensive spatiotemporal analysis of heatwave patterns at county-level across Mississippi over the past four decades, integrating diverse temperature datasets and heatwave indices. Our results demonstrate intensifying heatwave frequency and duration beyond natural fluctuations, with alarmingly high heat index values observed during events. Heatwave events have clearly become more prevalent and prolonged across both daytime and nighttime periods. An integrated HWRI revealed that certain regions face compounded threats from extreme heat and social vulnerability. Specifically, counties in northwest Mississippi emerged as hotspots based on combined physical exposure and sensitivity characteristics.

The African American communities in northwest Mississippi experience high poverty rates and maximum impacts, highlighting the need for targeted protections and support. This intersection of escalating heatwave hazards and socioeconomic disadvantage spotlights an environmental justice imperative for urgent targeted intervention. While peak single-event heatwave temperatures showed no detectable trend, the rising trending heatwave numbers and total heat days pose serious concern given their substantial public health and infrastructure impacts. Nighttime relief is diminishing, leading to concerning day–night persistence that eliminates crucial recovery periods. HWRI informs proactive measures and targeted resource allocation to mitigate associated risks. Our study can further support public health initiatives by informing interventions to protect vulnerable populations. Additionally, it guides urban planning decisions to create resilient infrastructure and green spaces. Ultimately, it enhances climate adaptation efforts by informing local policies and bolstering community resilience.

Data and code availability

All or part of the data and code will be made available upon request to the corresponding author. We used freely available codes such as Numpy, Pandas, Matplotlib, and Seaborn for data analysis and graph production.

Received: 29 February 2024; Accepted: 30 August 2024

Published online: 06 September 2024

References

- Perkins-Kirkpatrick, S. E. & Lewis, S. C. Increasing trends in regional heatwaves. *Nat. Commun.* **11**, 3357 (2020).
- Ghanbari, M., Arabi, M., Georgescu, M. & Broadbent, A. M. The role of climate change and urban development on compound dry-hot extremes across US cities. *Nat. Commun.* **14**, 3509 (2023).
- Lesk, C., Rowhani, P. & Ramankutty, N. Influence of extreme weather disasters on global crop production. *Nature* **529**, 84–87 (2016).
- Kapwata, T., Gebreslasie, M. T. & Wright, C. Y. An analysis of past and future heatwaves based on a heat-associated mortality threshold: Towards a heat health warning system. *Environ. Health* **21**, 112 (2022).
- Marx, W., Haunschild, R. & Bornmann, L. Heat waves: A hot topic in climate change research. *Theor. Appl. Climatol.* **146**, 781–800 (2021).
- Anderson, B. G. & Bell, M. L. Weather-related mortality: How heat, cold, and heat waves affect mortality in the United States. *Epidemiology* **20**, 205 (2009).
- Basu, R. & Samet, J. M. Relation between elevated ambient temperature and mortality: A review of the epidemiologic evidence. *Epidemiol. Rev.* **24**, 190–202 (2002).
- Gasparrini, A. *et al.* Temporal variation in heat-mortality associations: A multicountry study. *Environ. Health Perspect.* **123**, 1200–1207 (2015).
- Jay, O. *et al.* Reducing the health effects of hot weather and heat extremes: From personal cooling strategies to green cities. *Lancet* **398**, 709–724 (2021).
- Khosla, R., Jani, A. & Perera, R. Health risks of extreme heat. *BMJ* **375**, n2438 (2021).
- Nanayakkara, S., Wang, W., Cao, J., Wang, J. & Zhou, W. Analysis of urban heat island effect, heat stress and public health in Colombo, Sri Lanka and Shenzhen, China. *Atmosphere* **14**(5), 839. <https://doi.org/10.3390/atmos14050839> (2023).
- Leal Filho, W. *et al.* Addressing the urban heat islands effect: A cross-country assessment of the role of green infrastructure. *Sustainability* **13**, 753 (2021).
- Bai, X. *et al.* Identification, physical mechanisms and impacts of drought–flood abrupt alternation: a review. *Front. Earth Sci.* <https://doi.org/10.3389/feart.2023.1203603> (2023).
- Christian, J. Global flash droughts expected to increase in a warming climate. *ScienceDaily*. <https://www.sciencedaily.com/releases/2023/05/230526183216.htm> (2023).
- Awasthi, A., Vishwakarma, K. & Pattanayak, K. C. Retrospection of heatwave and heat index. *Theor. Appl. Climatol.* **147**, 589–604 (2022).
- Globe in 2020 | Copernicus. <https://climate.copernicus.eu/esotc/2020/globe-in-2020> (2020).
- Sanderson, K. Earth's average 2023 temperature is now likely to reach 1.5 °C of warming. *Nature* <https://doi.org/10.1038/d41586-023-02995-7> (2023).
- Shahzad, U. Global warming: Causes, effects and solutions. *Durreesamin J.* **1**(4), 1–7 (2015).
- Nugent, H. Here's how heat waves can impact economies, as well as people and wildlife. *World Econ. Forum* <https://www.weforum.org/agenda/2022/07/heat-waves-economy-climate-crisis/> (2022).
- Li, D., Yuan, J. & Kopp, R. E. Escalating global exposure to compound heat-humidity extremes with warming. *Environ. Res. Lett.* **15**, 064003 (2020).
- Mora, C. *et al.* Global risk of deadly heat. *Nat. Clim. Chang.* **7**, 501–506 (2017).
- Atlantic Council. *Extreme Heat: The Economic and Social Consequences for the United States*. <https://www.atlanticcouncil.org/in-depth-research-reports/report/extreme-heat-the-economic-and-social-consequences-for-the-united-states/> (2021).
- Thompson, V. *et al.* The most at-risk regions in the world for high-impact heatwaves. *Nat. Commun.* **14**, 2152 (2023).
- Chambers, J. Global and cross-country analysis of exposure of vulnerable populations to heatwaves from 1980 to 2018. *Clim. Chang.* **163**, 539–558 (2020).
- Meehl, G. A. & Tebaldi, C. More intense, more frequent, and longer lasting heat waves in the 21st century. *Science* **305**, 994–997 (2004).
- U.S. Global Change Research Program *et al.* *Climate Science Special Report: Fourth National Climate Assessment, Volume I*. <https://science2017.globalchange.gov/>. <https://doi.org/10.7930/J01964J6> (2017).
- Bailey, M. UW School of Public Health. <https://sph.washington.edu/news-events/news/warming-climate-may-lead-dramatic-increase-us-deaths-due-heat-exposure-study-shows> (2020).
- Ballester, J. *et al.* Heat-related mortality in Europe during the summer of 2022. *Nat. Med.* **29**, 1857–1866 (2023).
- US EPA. *US EPA - Technical Documentation - Heatwaves* (2021).
- Khatana. The Increasing Death Toll in the U.S. From Extreme Heat. *Time* <https://time.com/6198720/heatwave-health-death-toll/> (2022).
- Coronado, A. & Lozano, J. Deadly heat wave in the central US strains infrastructure, transportation and the Texas power grid. *AP News* <https://apnews.com/article/summer-heat-wave-fd19c3995992c93121ef4baedcbcf07e> (2023).
- Mathews, R. Heat Waves Cost to Infrastructure Add Up for State Governments | Aii. *Alliance for Innovation and Infrastructure* <https://www.aai.org/heat-wave-costs-to-infrastructure-add-up-for-state-governments/> (2021).
- US Government Publishing Office. *A Budget for a Better America*. <https://www.govinfo.gov/content/pkg/BUDGET-2020-BUD/pdf/BUDGET-2020-BUD.pdf> (2019).
- Kjellstrom, T., Freyberg, C., Lemke, B., Otto, M. & Briggs, D. Estimating population heat exposure and impacts on working people in conjunction with climate change. *Int. J. Biometeorol.* **62**, 291–306 (2018).
- Zhang, Y. & Shindell, D. T. Costs from labor losses due to extreme heat in the USA attributable to climate change. *Clim. Chang.* **164**, 35 (2021).
- Klingelhöfer, D., Braun, M., Brüggmann, D. & Groneberg, D. A. Heatwaves: does global research reflect the growing threat in the light of climate change?. *Glob. Health* **19**, 56 (2023).
- Choi, E. Y., Lee, H. & Chang, V. W. Cumulative exposure to extreme heat and trajectories of cognitive decline among older adults in the USA. *J. Epidemiol. Commun. Health* **77**, 728–735 (2023).
- Liss, A. & Naumova, E. N. Heatwaves and hospitalizations due to hyperthermia in defined climate regions in the conterminous USA. *Environ. Monit. Assess.* **191**, 1–16 (2019).
- US EPA, O. EPA Report Shows Disproportionate Impacts of Climate Change on Socially Vulnerable Populations in the United States. <https://www.epa.gov/newsreleases/epa-report-shows-disproportionate-impacts-climate-change-socially-vulnerable> (2021).
- Vaidyanathan, A. Heat-related deaths—United States, 2004–2018. *MMWR Morb. Mortal. Wkly. Rep.* **69**, 729–734 (2020).

41. CDC. Heat and the Low Income | Natural Disasters and Severe Weather | CDC. <https://www.cdc.gov/disasters/extremeheat/lowincome.html> (2020).
42. Gronlund, C. J. Racial and socioeconomic disparities in heat-related health effects and their mechanisms: A review. *Curr. Epidemiol. Rep.* **1**, 165–173 (2014).
43. Muyskens, J., Tran, A. B., Phillips, A., Ducroquet, S. & Ahmed, N. More dangerous heat waves are on the way: See the impact by Zip code. *Washington Post* <https://www.washingtonpost.com/climate-environment/interactive/2022/extreme-heat-risk-map-us/> (2023).
44. Witze, A. Extreme heatwaves: Surprising lessons from the record warmth. *Nature* **608**, 464–465 (2022).
45. IPCC. Climate change widespread, rapid, and intensifying—IPCC—IPCC. <https://www.ipcc.ch/2021/08/09/ar6-wg1-20210809-pr/> (2021).
46. Baranyai, E. & Banai, Á. Heat projections and mortgage characteristics: Evidence from the USA. *Clim. Chang.* **175**, 14 (2022).
47. Bastin, J.-F. *et al.* Understanding climate change from a global analysis of city analogues. *PLOS ONE* **14**, e0217592 (2019).
48. Liu, L. & Qin, X. Analysis of heatwaves based on the universal thermal climate index and apparent temperature over mainland Southeast Asia. *Int. J. Biometeorol.* <https://doi.org/10.1007/s00484-023-02562-9> (2023).
49. Marcotullio, P. J., Kefler, C. & Fekete, B. M. Global urban exposure projections to extreme heatwaves. *Front. Built Environ.* <https://doi.org/10.3389/fbuil.2022.947496> (2022).
50. Blanks, J., Abuabara, A., Roberts, A. & Semien, J. Preservation at the intersections: Patterns of disproportionate multihazard risk and vulnerability in Louisiana's historic African American cemeteries. *Environ. Justice* **14**, 1–13 (2021).
51. Jankowski, K. J. & Converse, D. L. Impacts of climate change on the Mississippi River | Wisconsin Initiative on Climate Change Impacts 2021 Assessment Report. *Wisconsin Initiative on Climate Change Impacts* <https://wicci.wisc.edu/2021-assessment-report/water/impacts-of-climate-change-on-the-mississippi-river/> (2022).
52. Team, I. W. D. Mississippi Climate. *Department of Geosciences at Mississippi State University* <https://www.geosciences.msstate.edu/state-climatologist/climate/> (2015).
53. StatsAmerica. Rank List: States in Profile. https://www.statsamerica.org/sip/rank_list.aspx?rank_label=pcpi1 (2022).
54. US Census Bureau. Census Bureau Tables. <https://data.census.gov/table?g=040XX00US28> (2020).
55. Muñoz-Sabater, J. *et al.* ERA5-Land: A state-of-the-art global reanalysis dataset for land applications. *Earth Syst. Sci. Data* **13**, 4349–4383 (2021).
56. Meteostat. meteostat: Access and analyze historical weather and climate data with Python. (2023).
57. Hersbach, H. *et al.* The ERA5 global reanalysis. *Q. J. R. Meteorol. Soc.* **146**(730), 1999–2049. <https://doi.org/10.1002/qj.3803> (2020).
58. Jiao, D., Xu, N., Yang, F. & Xu, K. Evaluation of spatial-temporal variation performance of ERA5 precipitation data in China. *Sci. Rep.* **11**(1), 17956. <https://doi.org/10.1038/s41598-021-97432-y> (2021).
59. Muñoz-Sabater, J. *et al.* ERA5-Land: A state-of-the-art global reanalysis dataset for land applications. *Earth Syst. Sci. Data* **13**(9), 4349–4383. <https://doi.org/10.5194/essd-13-4349-2021> (2021).
60. Tarek, M., Brissette, F. P. & Arseneault, R. Evaluation of the ERA5 reanalysis as a potential reference dataset for hydrological modeling over North America. *Hydrol. Earth Syst. Sci.* **24**(5), 2527–2544. <https://doi.org/10.5194/hess-24-2527-2020> (2020).
61. Rathi, S. K., Chakraborty, S., Mishra, S. K., Dutta, A. & Nanda, L. A heat vulnerability index: Spatial patterns of exposure, sensitivity and adaptive capacity for urbanites of four cities of India. *Int. J. Environ. Res. Public Health* **19**, 283 (2021).
62. Xu, Y., Hong, T., Zhang, W., Zeng, Z. & Wei, M. Heat vulnerability index development and mapping (2021).
63. Arsad, F. S. *et al.* The impact of heatwaves on mortality and morbidity and the associated vulnerability factors: A systematic review. *Int. J. Environ. Res. Public Health* **19**, 16356 (2022).
64. CDC/ATSDR. CDC/ATSDR Social Vulnerability Index (SVI). <https://www.atsdr.cdc.gov/placeandhealth/svi/index.html> (2023).
65. Abatzoglou, J. T. Development of gridded surface meteorological data for ecological applications and modelling. *Int. J. Climatol.* **33**, 121–131 (2013).
66. Sen, P. K. Estimates of the regression coefficient based on Kendall's Tau. *J. Am. Stat. Assoc.* **63**, 1379–1389 (1968).
67. Kendall, M. Rank Correlation Methods. By Maurice G. Kendall, M.A. [Pp. vii + 160. London: Charles Griffin and Co. Ltd., 42 Drury Lane, 1948. 18s.]. *J. Inst. Actuar.* **75**, 140–141 (1948).
68. Mann, H. B. Nonparametric tests against trend. *Econometrica* **13**, 245 (1945).
69. Hussain, M. M. & Mahmud, I. pyMannKendall: A python package for non parametric Mann Kendall family of trend tests. *J. Open Source Softw.* **4**, 1556 (2019).
70. Pedregosa, F. *et al.* Scikit-learn: Machine Learning in Python. *Mach. Learn. Python* **12**, 2825 (2011).
71. Rothfus, L. P. The Heat Index 'Equation' (or, More Than You Ever Wanted to Know About Heat Index). (1990).
72. Anderson, G. B., Bell, M. L. & Peng, R. D. Methods to calculate the heat index as an exposure metric in environmental health research. *Environ. Health Perspect.* **121**, 1111–1119 (2013).
73. Opitz-Stapleton, S. *et al.* Heat index trends and climate change implications for occupational heat exposure in Da Nang, Vietnam. *Clim. Serv.* **2–3**, 41–51 (2016).
74. WHO. Heat and Health. <https://www.who.int/news-room/fact-sheets/detail/climate-change-heat-and-health> (2018).
75. Silveira, I. H., Cortes, T. R., Bell, M. L. & Junger, W. L. Effects of heat waves on cardiovascular and respiratory mortality in Rio de Janeiro, Brazil. *PLOS ONE* **18**, e0283899 (2023).
76. Anderson, B. G. & Bell, M. L. Heat Waves in the United States: Mortality Risk during Heat Waves and Effect Modification by Heat Wave Characteristics in 43 U.S. Communities. <https://ehp.niehs.nih.gov/doi/epdf/https://doi.org/10.1289/ehp.1002313> (2011).
77. ASCE. How to make infrastructure more resilient against climate change. <https://www.asce.org/publications-and-news/civil-engineering-source/civil-engineering-magazine/issues/magazine-issue/article/2022/01/how-to-make-infrastructure-more-resilient-against-climate-change> (2022).
78. Simeï, W., Liu, X. & He, B.-J. Impact of Urban Overheating on Critical Infrastructure. In *Climate Change and Environmental Sustainability* (eds He, B.-J. *et al.*) 83–89 (Springer, 2022). https://doi.org/10.1007/978-3-031-12015-2_9.
79. Ioannou, L. G. *et al.* Occupational heat stress: Multi-country observations and interventions. *Int. J. Environ. Res. Public Health* **18**, 6303 (2021).
80. Kjellstrom, T. *et al.* Heat, human performance, and occupational health: A key issue for the assessment of global climate change impacts. *Annu. Rev. Public Health* **37**, 97–112 (2016).
81. Chan, A. P. C. & Yi, W. Heat stress and its impacts on occupational health and performance. *Indoor Built Environ.* **25**, 3–5 (2016).
82. Somogyi, T. & Nagy, R. Some impacts of global warming on critical infrastructure protection-heat waves and the European financial sector. *Insights Reg. Dev.* **4**, 11–20 (2022).
83. U.S. Census Bureau QuickFacts: Yalobusha County, Mississippi. <https://www.census.gov/quickfacts/fact/table/yalobushacountymississippi/PST045222> (2022).
84. U.S. Census Bureau QuickFacts: George County, Mississippi. <https://www.census.gov/quickfacts/fact/table/georgecountymississippi/PST045222> (2022).
85. NWS. Beat the Heat, Check the Backseat. <https://www.weather.gov/crp/beattheheat> (2014).
86. Pathmeswaran, C., Sen Gupta, A., Perkins-Kirkpatrick, S. E. & Hart, M. A. Exploring potential links between co-occurring coastal terrestrial and marine heatwaves in Australia. *Front. Clim.* **4**, 792730 (2022).
87. Hu, L. A global assessment of coastal marine heatwaves and their relation with coastal urban thermal changes. *Geophys. Res. Lett.* **48**, e2021GL093260 (2021).

88. Yu, Z. *et al.* Critical review on the cooling effect of urban blue-green space: A threshold-size perspective. *Urban For. Urban Green.* **49**, 126630 (2020).

Acknowledgements

This research is supported by the Hydrological Impacts Computing, Outreach, and Resiliency Partnership (HICORPS) Project, in collaboration with the U.S. Army Engineer Research and Development Center (ERDC) and WOOLPERT. We would like to acknowledge the Department of Civil and Environmental Engineering, Jackson State University, for providing computing facilities in Hydraulic Lab to conduct this research.

Author contributions

Credit Author Statement: S.B.: Conceptualization, Methodology, Writing- Original Draft, Data Curation, Formal Analysis, Figures S.B.: Writing-Review & Editing, S.S.: Writing – Review & Editing, Supervision, L.D.W.: Funding acquisition, Supervision F.A.: Funding acquisition, Supervision R.T.: Conceptualization, Methodology, Writing – Original Draft, Supervision, Resources. All authors reviewed this manuscript.

Competing interests

The authors declare no competing interests.

Additional information

Supplementary Information The online version contains supplementary material available at <https://doi.org/10.1038/s41598-024-71704-9>.

Correspondence and requests for materials should be addressed to S.B.

Reprints and permissions information is available at www.nature.com/reprints.

Publisher's note Springer Nature remains neutral with regard to jurisdictional claims in published maps and institutional affiliations.

Open Access This article is licensed under a Creative Commons Attribution-NonCommercial-NoDerivatives 4.0 International License, which permits any non-commercial use, sharing, distribution and reproduction in any medium or format, as long as you give appropriate credit to the original author(s) and the source, provide a link to the Creative Commons licence, and indicate if you modified the licensed material. You do not have permission under this licence to share adapted material derived from this article or parts of it. The images or other third party material in this article are included in the article's Creative Commons licence, unless indicated otherwise in a credit line to the material. If material is not included in the article's Creative Commons licence and your intended use is not permitted by statutory regulation or exceeds the permitted use, you will need to obtain permission directly from the copyright holder. To view a copy of this licence, visit <http://creativecommons.org/licenses/by-nc-nd/4.0/>.

© The Author(s) 2024